

Energy-Specific Bethe-Salpeter Equation Implementation for Efficient Optical Spectrum Calculations

Christopher Hillenbrand, Jiachen Li, and Tianyu Zhu^{a)}

*Department of Chemistry, Yale University, New Haven, Connecticut 06520,
United States*

We present an energy-specific Bethe-Salpeter equation (BSE) implementation for efficient core and valence optical spectrum calculations. In energy-specific BSE, high-lying excitation energies are obtained by constructing trial vectors and expanding the subspace targeting excitation energies above the predefined energy threshold in the Davidson algorithm. To calculate optical spectra over a wide energy range, energy-specific BSE can be applied to multiple consecutive small energy windows, where trial vectors for each subsequent energy window are made orthogonal to the subspace of preceding windows to accelerate the convergence of the Davidson algorithm. For seven small molecules, energy-specific BSE combined with G_0W_0 provides small errors around 0.8 eV for absolute and relative K -edge excitation energies when starting from a hybrid PBEh solution with 45% exact exchange. We further showcase the computational efficiency of this approach by simulating the $N 1s$ K -edge excitation spectrum of the porphine molecule and the valence optical spectrum of silicon nanoclusters involving 5,000 excited states using G_0W_0 -BSE. This work expands the applicability of the GW -BSE formalism for investigating high-energy excited states of large systems.

^{a)}Electronic mail: tianyu.zhu@yale.edu

I. INTRODUCTION

Accurate description of excited states plays a crucial role in understanding various phenomena and processes in chemistry, biochemistry, and materials science, such as charge transfer in photoinduced reactions¹⁻⁵ and quantum confinement in nanoparticles^{6,7}. Spectroscopy, in its numerous flavors, offers some of the best available means to manipulate and observe excited states. As investigators propose ever more ambitious experiments, establishing the link between the experimental data and the underlying physical phenomena will accordingly become more difficult. Therefore, simulating excited-state properties with first-principle approaches can assist in the interpretation of experimental data and also aid in the design of new experiments.

Of the many quantum chemistry methods have been developed to compute excited-state properties, time-dependent density functional theory (TDDFT)⁸⁻¹⁰ is the most popular, having been widely implemented in modern quantum chemistry packages. With the Davidson algorithm¹¹, the computational cost of TDDFT scales as $O(N^4)$, where N is the size of the system. Because of the good balance between computational cost and accuracy, TDDFT has achieved great success in simulating excited states to model excited-state properties of molecules, liquids and solid-state materials¹²⁻¹⁸. However, TDDFT suffers from several shortcomings. For example, it is well known that TDDFT with conventional exchange-correlation (XC) functionals fails to describe charge-transfer and Rydberg excited states due to the incorrect long-range behavior^{19,20}, and it has an undesired dependence on the choice of the XC functional. Recently, the orbital-optimized DFT approach has been shown to outperform TDDFT for predicting excitation energies^{21,22}. Other linear-response and wave function based methods have been developed to improve over TDDFT, such as the particle-particle random phase approximation (ppRPA)²³⁻³¹, non-orthogonal configuration interaction singles (NOCIS)^{32,33}, equation-of-motion coupled-cluster (EOM-CC)³⁴⁻³⁸ theory, and algebraic diagrammatic construction (ADC)^{37,39-43}.

Another alternative to TDDFT is the Bethe-Salpeter equation⁴⁴⁻⁴⁶ (BSE) formalism in the Green's function theory^{47,48}, which has been widely used to simulate optical spectroscopy for a broad range of systems⁴⁹⁻⁶⁴. BSE usually takes quasiparticle (QP) energies computed at the GW level as the input, denoted as GW -BSE. The success of the GW -BSE approach can be attributed to several reasons. First, the screened interaction formulated with QP energies from the GW calculation is important to describe the electron-hole interaction in realistic systems^{65,66}. Second, GW QP energies substantially improve upon the Kohn-Sham orbital energies in DFT⁶⁷⁻⁶⁹ for

predicting both core and valence energy levels, which are the critical quantities to calculate optical excitation energies. Third, the scaling of BSE is $O(N^4)$ by using the standard Davidson algorithm⁷⁰, which is computationally affordable. To reduce the cost of the computational bottleneck *GW* step, various machine learning models have recently been proposed to obtain QP energies^{71–74}. BSE can also leverage recent developments of DFT by using orbital energies from generalized Kohn-Sham approaches to bypass the computationally demanding *GW* calculations^{57,75}. Parallel to *GW*-BSE, BSE formulated with the T-matrix self-energy has also been developed^{76,77}.

Despite the success of the *GW*-BSE formalism, it still faces several challenges. First, predicting high-lying excitations, such as core excitations as measured in X-ray absorption spectroscopy (XAS), can be difficult for *GW*-BSE using the standard Davidson algorithm, because the required subspace is extremely large compared to those for low-lying excitations. As shown in Ref. 78, full diagonalization of the BSE matrix was used to access *K*-edge excitation energies, which scales as $O(N^6)$ and is computationally prohibitive for large systems. Second, computing optical spectra for large systems (e.g., nanoclusters) in a wide energy range with fine resolution requires solving for a massive number of excited states simultaneously⁷⁹, which leads to a large subspace in the Davidson algorithm and considerably degrades computational efficiency. To address this issue, filter-diagonalization^{80,81} and stochastic time-dependent propagation^{82,83} approaches have been developed.

In this work, we present an efficient energy-specific *GW*-BSE approach, aiming to compute high-lying core excitation energies and optical spectra with dense excited-state energy levels. The energy-specific technique has been employed in TDDFT and EOM-CCSD approaches for calculating *K*-edge excitation energies^{84–87}. Here we combine the energy-specific technique with the *GW*-BSE formalism and further develop an efficient algorithm for solving BSE in multiple energy windows. In the energy-specific BSE approach, trial vectors targeting excitation energies above the predefined energy threshold are constructed for the Davidson algorithm, then the subspace is expanded with new trial vectors associated with transitions above the target energy threshold. To improve the efficiency of solving BSE for multiple energy windows, trial vectors orthogonal to the true eigenvectors solved preceding energy windows are constructed for the subsequent energy window. By applying energy-specific BSE to multiple small energy windows, optical spectra over a wide energy range can be obtained, which shares the similar idea of employing small time windows in real-time TDDFT⁷⁹. We first demonstrate that energy-specific *GW*-BSE predicts accurate *K*-edge excitation energies of small molecules and the porphine molecule, requiring only similar

computational cost to low-lying excited-state calculations. Then we show that the energy-specific GW -BSE approach is capable of simulating optical spectra in a wide energy range for silicon nanoclusters, which involves thousands of excited states.

II. THEORY

A. Bethe-Salpeter equation

In the GW -BSE approach, the BSE kernel in the Dyson equation for the two-particle correlation function is the functional derivative of the GW self-energy with respect to the one-particle Green's function, which expresses the linear response of the one-particle Green's function to a general non-local perturbation and leads to the dynamical screened interaction^{48,9,10}, the Bethe-Salpeter equation is a linear response eigenvalue problem^{66,70,88–90}

$$\begin{bmatrix} \mathbf{A} & \mathbf{B} \\ \mathbf{B}^\dagger & \mathbf{A}^\dagger \end{bmatrix} \begin{bmatrix} X \\ Y \end{bmatrix} = \Omega \begin{bmatrix} \mathbf{I} & 0 \\ 0 & -\mathbf{I} \end{bmatrix} \begin{bmatrix} X \\ Y \end{bmatrix} \quad (1)$$

where Ω is the excitation energy and X and Y are the transition amplitudes. The matrices A and B are defined as

$$A_{ia,jb} = \delta_{ij}\delta_{ab}(\varepsilon_a - \varepsilon_i) + v_{ia,jb} - W_{ij,ab} \quad (2)$$

$$B_{ia,jb} = v_{ia,bj} - W_{ib,aj} \quad (3)$$

where $\{\varepsilon_p\}$ are quasiparticle energies computed at the GW level. For clarity, we will also assume that A and B are both real and symmetric. This is the case if the orbitals are real. In Eq. 2 and the following, we use i, j, k, l for occupied orbitals, a, b, c, d for virtual orbitals, p, q, r, s for general molecular orbitals, and m for the index of excited states. In Eq. 1, v is the Coulomb interaction defined as $v_{pq,rs} = \int dx_1 dx_2 \phi_p^*(x_1)\phi_q(x_1)||r_1 - r_2||^{-1}\phi_r^*(x_2)\phi_s(x_2)$, and W is the screened interaction taken at the static limit ($\omega = 0$). In turn, W is given by

$$W_{pq,rs} = \sum_{tu} (\epsilon^{-1})_{pq,tu} v_{tu,rs} \quad (4)$$

where the dielectric function ϵ is calculated from the static response function χ ^{70,90}

$$\epsilon_{pq,rs} = \delta_{pr}\delta_{qs} - v_{pq,rs} \chi_{rs,rs}, \quad (5)$$

$$\chi_{ia,ia} = \chi_{ai,ai} = (\varepsilon_i - \varepsilon_a)^{-1} \quad (6)$$

BSE going beyond the static limit allows the access to double excitations^{91,92}. The Tamm-Dancoff approximation (TDA) in BSE is obtained by taking $B \approx 0$ in Eq. 1. As shown in Refs. 93–95, *GW*-BSE/TDA can lead to blue-shifts in nanosized systems and worse estimations for singlet-triplet gaps in organic molecules. With excitation energies and transition amplitudes obtained from Eq. 1, the oscillator strength of the m -th excited state is computed as

$$f_m = \frac{2}{3} \Omega_m \sum_{r=x,y,z} \left[\sum_{ia} \langle i | \hat{r} | a \rangle (X_{ia}^m + Y_{ia}^m) \right]^2 \quad (7)$$

The only difference in Eq. 1 compared to the Casida equation in TDDFT is that the BSE kernel replaces the XC kernel. A full diagonalization of Eq. 1 scales as $O(N^6)$. If only low-lying excited states are desired, Eq. 1 can be solved with the canonical Davidson algorithm¹¹ with $O(N^4)$ scaling. However, the computational efficiency significantly degrades when the number of desired roots becomes large.

B. Energy-Specific BSE

1. Computational method

In practice, to reduce the computational cost, Eq. 1 is usually rewritten as a generalized symmetric eigenproblem of half the dimension^{11,89}

$$(\mathbf{A} - \mathbf{B})(\mathbf{A} + \mathbf{B}) (X + Y) = \Omega^2(X + Y) \quad (8)$$

where $\mathbf{A} + \mathbf{B}$ and $\mathbf{A} - \mathbf{B}$ are symmetric positive definite^{11,96}. Unless the entire spectrum is needed, extracting a small fraction of eigenpairs with a matrix-free solver is usually faster than full diagonalization of $(\mathbf{A} - \mathbf{B})(\mathbf{A} + \mathbf{B})$. Because such methods avoid explicitly constructing \mathbf{A} and \mathbf{B} , they can also take advantage of any available cost-saving approximations to v and W matrices in Eq. 2 and Eq. 3, such as Cholesky decomposition of the electron repulsion integrals (used in this work). Traditionally, the Davidson algorithm^{11,97} (Algorithm 1) is used for solving TDDFT and BSE problems of the form in Eq. 1.

Algorithm 1 Davidson algorithm for linear response^{11,97}

Require: An orthonormal list of starting vectors $\mathbf{U} = [u_1 \cdots u_k]$, a convergence tolerance $\tau > 0$, and the number of desired roots $N \leq k$.

- 1: **while** not converged **do**
 - 2: Calculate $(\mathbf{A} + \mathbf{B})\mathbf{U}$, $(\mathbf{A} - \mathbf{B})\mathbf{U}$ for any new vectors in U .
 - 3: Form the matrices $\tilde{\mathbf{K}} \leftarrow \mathbf{U}^\dagger(\mathbf{A} + \mathbf{B})\mathbf{U}$ and $\tilde{\mathbf{M}} \leftarrow \mathbf{U}^\dagger(\mathbf{A} - \mathbf{B})\mathbf{U}$.
 - 4: Solve⁹⁸ $\tilde{\mathbf{M}}\tilde{\mathbf{K}}(\tilde{X} + \tilde{Y}) = \Omega^2(\tilde{X} + \tilde{Y})$ for N lowest eigenvalues Ω_i and right eigenvectors $\tilde{X}_i + \tilde{Y}_i$.
 - 5: Calculate the left eigenvectors $\tilde{X}_i - \tilde{Y}_i \leftarrow \tilde{\mathbf{K}}(\tilde{X}_i + \tilde{Y}_i)/\Omega_i$
 - 6: Obtain the approximate eigenvectors (Ritz vectors) of $(\mathbf{A} - \mathbf{B})(\mathbf{A} + \mathbf{B})$ in the MO space:
$$X_i - Y_i = \mathbf{U}(\tilde{X}_i - \tilde{Y}_i), \quad X_i + Y_i = \mathbf{U}(\tilde{X}_i + \tilde{Y}_i) \quad \text{for all } i$$
 - 7: Calculate the residues $L_i \leftarrow (\mathbf{A} - \mathbf{B})\mathbf{U}(\tilde{X}_i - \tilde{Y}_i) - \Omega_i(X_i + Y_i)$, $R_i \leftarrow (\mathbf{A} + \mathbf{B})\mathbf{U}(\tilde{X}_i + \tilde{Y}_i) - \Omega_i(X_i - Y_i)$.
 - 8: Initialize \mathbf{Q} to an empty list [].
 - 9: **for** $i = 1, \dots, N$ **do**
 - 10: **if** either $\|L_i\|$ or $\|R_i\|$ exceeds the convergence tolerance τ **then**
 - 11: Add the preconditioned residues $(\Omega_i - (\varepsilon_a - \varepsilon_i))^{-1}L_i$ and $(\Omega_i - (\varepsilon_a - \varepsilon_i))^{-1}R_i$ to \mathbf{Q} .
 - 12: **end if**
 - 13: **end for**
 - 14: **if** \mathbf{Q} is empty **then**
 - 15: Get \mathbf{X}' and \mathbf{Y}' from $\mathbf{X}' + \mathbf{Y}'$ and $\mathbf{X}' - \mathbf{Y}'$ and **return** $\{\Omega, \mathbf{X}', \mathbf{Y}'\}$.
 - 16: **end if**
 - 17: Orthonormalize the vectors of \mathbf{Q} against \mathbf{U} and among themselves⁹⁹; then add them to \mathbf{U} .
 - 18: **end while**
-

In Ref. 84, Liang et. al. employed an energy screening and bracketing technique to solve the Casida equations for higher-lying states in TDHF/TDDFT. Because the BSE and Casida equations are both of the form in Eq. 1, this technique can be easily generalized to this context. Aside from the matter of the initial trial vectors U , it requires only one modification to Algorithm 1, as shown in Algorithm 2. In this way, only Ritz pairs above a given energy minimum are expanded. Note that the modified algorithm is equivalent to the original Davidson algorithm if $E_{\min} = 0$.

Algorithm 2 Energy-specific Davidson is the same as algorithm 1 except

Require: An energy minimum E_{\min} .

- **Line 4:** Solve the generalized symmetric eigenproblem $\tilde{\mathbf{M}}\tilde{\mathbf{K}}(\tilde{X} + \tilde{Y}) = \Omega^2(\tilde{X} + \tilde{Y})$ for N lowest eigenvalues Ω_i and right eigenvectors $\tilde{X}_i + \tilde{Y}_i$. Supposing that only states above an energy minimum E_{\min} are sought, an eigenpair Ω^2 , $\tilde{X} + \tilde{Y}$ is **discarded** if $\Omega < E_{\min}$.
-

When calculating core excitation energies, the desired states are sometimes interspersed with unwanted states that lie in the same energy region. The energy bracketing tactic of Algorithm 2 cannot discriminate between core and non-core excitations, and will be inefficient if the unwanted states are numerous and narrowly spaced. We encountered this issue in our calculation of porphine N K -edge energies, and found that a simple modification to Algorithm 2 reduced the cost of this particular calculation by a large factor, as shown in Algorithm 3. This modification has no impact on the accuracy of the excited states returned by the algorithm, since convergence is verified the same way as in Algorithm 1.

Algorithm 3 Core-specific Davidson is the same as algorithm 2 except

Require: A list of occupied orbitals O for which excitations are sought, and a threshold τ_{occ} .

- **Line 10:** The residues of X, Y are added to \mathbf{Q} if $\|L\| > \tau$ or $\|R\| > \tau$, **but only if**

$$\sum_{o \in O} \sum_a X_{oa}^2 > \tau_{\text{occ}},$$

i.e., the total weight of O in X is large enough.

- **Line 15:** Only return a Ritz pair Ω, X, Y if $\sum_{o \in O} \sum_a X_{oa}^2 > \tau_{\text{occ}}$.
-

2. Initial trial vector generation

Although it is possible to use random starting vectors \mathbf{U} , our implementation chooses them as follows. Given a list of occupied orbitals O , all pairs (o, a) , $o \in O$ below the energy minimum (plus a shift $\delta E \geq 0$), i.e., those with $\varepsilon_a - \varepsilon_o < E_{\min} + \delta E$, are discarded. Finally, for each of the k lowest energy remaining pairs, the elementary vector representing the $o \rightarrow a$ transition is added to \mathbf{U} . This is the same method used by Liang et. al. in Ref. 84, except that the starting vectors can be restricted, if necessary, to a given list of occupied orbitals. For all core K -edge calculations in this

paper, O is set to those occupied MOs with a minimum of 30% $1s$ orbital character on the target atoms.

3. *Restarts, deflation, and sliding windows*

During a calculation, it sometimes happens that $\tilde{\mathbf{M}} = \mathbf{U}^\dagger(\mathbf{A} - \mathbf{B})\mathbf{U}$ is non-positive due to loss of orthogonality among the vectors of \mathbf{U} . When this occurs, Algorithm 1 cannot proceed, and restarting is necessary. During a restart, a new orthonormal basis \mathbf{U}' is constructed from the Ritz vectors \mathbf{X}' and \mathbf{Y}' found in the previous iteration. Then \mathbf{U}' replaces \mathbf{U} , and the algorithm restarts at line 1.

Because recalculating $(\mathbf{A} + \mathbf{B})\mathbf{U}$ and $(\mathbf{A} - \mathbf{B})\mathbf{U}$ is very costly, it is important to avoid restarts. To prevent loss of orthogonality, our implementation orthogonalizes the new search vectors $[q_1 \cdots q_N]$ against \mathbf{U} twice—both before and after orthogonalizing the q_i among themselves—before adding them to \mathbf{U} in line 17. Thanks to this, unintentional restarts rarely occur.

As a calculation proceeds, the search space can grow very large, and the cost of solving the eigenproblems within each iteration can exceed that of the (usually more costly) contraction step. When the search space grows too large, it is deflated via an automatic restart that discards most of the Ritz vectors, as above.

Combined with a sliding window method, energy-specific bracketing is also useful when one wishes to obtain as many excited states as possible in a progressive fashion, without committing to a specific number of states. In this variation of Algorithm 2, the first several (20–50) states above E_{\min} are converged and saved. The energy minimum E_{\min} is then reset to lie just above the highest converged state, and the solver moves onto the next window. Without a time limit, this algorithm runs indefinitely or until failure. Two kinds of failure have been observed:

1. If the solver keeps only Ritz vectors from (or surrounding) the current energy window during deflation, subsequent iterations take longer to converge until, eventually, no progress occurs between deflations.
2. If the solver keeps all Ritz vectors in the current window and below, steady progress continues until memory runs out or the cost of diagonalizing $\tilde{\mathbf{M}}\tilde{\mathbf{K}}$ becomes overwhelming.

The sliding window technique is employed in this work only for calculating the silicon nanocluster valence spectrum.

III. COMPUTATIONAL DETAILS

We implemented the energy-specific BSE approach in the fcDMFT library^{100–103}, a quantum embedding library based on the PySCF quantum chemistry software package^{104,105}. All ground-state DFT calculations were carried out using PySCF. GW ^{106,107} without density fitting. GW and BSE calculations were performed with fcDMFT, using Cholesky-decomposed ERIs generated by PySCF. For each basis set, the corresponding RIFIT auxiliary basis set was used if available; otherwise an RI auxiliary basis was generated with the AutoAux algorithm^{108,109} or PySCF (in the case of porphine). All GW and DFT calculations were non-relativistic. A post- GW -BSE correction scheme derived in Ref. 110 was employed for relativistic corrections to the K -edge excitation energies. The magnitude of the corrections increase with the atomic number: 0.12 eV for $C1s$, 0.24 for $N1s$ and 0.42 eV for $O1s$.

In the calculations for K -edge excitation energies of seven small molecules including NH_3 , CH_2O , CO , N_2 , N_2O , C_2H_4 and H_2O , geometries were optimized at the CCSD level with the def2-TZVPD basis set¹¹¹ with GAUSSIAN16 A.03¹¹². XAS experiment reference values were taken from Ref. 85. For subsequent DFT and GW -BSE calculations, aug-cc-pVQZ basis set¹¹³ was used for H and the aug-cc-pCVQZ basis set¹¹⁴ was used for remaining atoms. G_0W_0 self-energy elements for the seven small molecules were evaluated analytically¹¹⁵ to obtain QP energies, where G_0W_0 was performed on top of the hybrid PBEh solutions with 45% exact exchange (denoted as PBEh45)^{78,116–118}. In energy-specific BSE calculations, the energy thresholds 280 eV, 390 eV, and 530 eV were used for C, N, and O K -edge excitation energies respectively.

In the calculations for K -edge excitation energies of porphine, the geometry was optimized at the B3LYP+D3 level^{119–121} with the 6-31G(d) basis set¹²² in GAUSSIAN16 A.03¹¹². XAS experiment reference values were taken from Refs. 123,124. For subsequent DFT and GW -BSE calculations, the aug-cc-pCVTZ basis set¹¹⁴ was used for N atoms, the cc-pVDZ basis set¹¹³ was used for C atoms, and the aug-cc-pVDZ basis set was used for H atoms. To reduce the computational cost, $G_0W_0@PBEh45$ self-energy elements of occupied orbitals were evaluated with the contour deformation technique^{106,116} that scales as $O(N^5)$, while self-energy elements of virtual orbitals were evaluated with the analytic continuation technique^{106,116} that scales as $O(N^4)$. In energy-specific BSE calculations, the energy threshold 397 eV was used to get N K -edge excitation energies.

In the calculation of valence spectrum of the silicon nanocluster, geometries was taken from

Ref. 72. Experiment optical gap was taken from Ref. 125. The cc-pVTZ basis set¹¹³ was used, and G_0W_0 quasiparticle energies were calculated using Padé analytic continuation and the diagonal approximation. In the BSE calculation, the MO space was truncated to include only orbitals with QP energies in the range $[-81.6, E_{\text{LUMO}} + 27.2]$ eV, and the Tamm-Dancoff approximation was used. The lowest lying 5000 excited states were obtained with the sliding window technique of Section II B 3. After obtaining oscillator strengths via Eq. 7, the optical absorption spectrum was plotted with Gaussian broadening ($\sigma = 0.05$ eV). For comparison, the optical absorption spectrum was also calculated with the Lanczos / generalized averaged Gauss quadrature method described in Ref. 96. To obtain the isotropic absorption spectrum, the three Cartesian components of the MO electric dipole moment were used as starting vectors in three runs of 500 iterations each; the spectra thus obtained were averaged¹²⁶.

IV. RESULTS

A. Benchmark of the Energy-Specific GW -BSE Approach

TABLE I. Excitation energies and oscillator strengths of H_2O and NH_3 obtained from G_0W_0 -BSE@PBEh45. aug-cc-pVQZ basis set was used for H and aug-cc-pCVQZ basis set was used for remaining atoms. Excitation energies are in eV and oscillator strengths are in A.U.

		energy-specific		full diagonalization	
		excitation energy	oscillator strength	excitation energy	oscillator strength
H_2O	$1s \rightarrow 4a_1/3s$	532.44	0.0168	532.43	0.0167
	$1s \rightarrow 2b_1/3p$	534.14	0.0363	534.14	0.0364
	$1s \rightarrow 3p (b_2)$	536.53	0.0163	536.53	0.0163
NH_3	$1s \rightarrow 3s$	399.65	0.0088	399.65	0.0088
	$1s \rightarrow 3p (E)$	401.28	0.0337	401.28	0.0337
	$1s \rightarrow 3p (A_1)$	401.28	0.0337	401.28	0.0337
	$1s \rightarrow 4s (A_1)$	402.70	0.0132	402.70	0.0132

We first benchmark the accuracy of the energy-specific GW -BSE approach. The calculated K -edge excitation energies and oscillator strengths obtained from energy-specific and full-diagonalization GW -BSE are shown in Table I. The excitation energies and oscillator strengths for

high-energy K -edge excitations from energy-specific Davidson are nearly identical to those from full diagonalization; the largest difference between the two is < 0.01 eV for excitation energies and < 0.0001 A.U. for oscillator strengths.

B. K -edge Excitation Energies

TABLE II. Mean absolute errors of absolute and relative K -edge excitation energies for 31 states of 7 small molecules obtained from different approaches. G_0W_0 -BSE/TDA@PBEh45 (literature) calculated with aug-cc-pCV6Z basis set were taken from Ref. 78. Results of TDDFT and EOM approaches calculated with d-aug-cc-pCVDZ basis set were taken from Ref. 85. Relativistic effects were considered using a post- GW -BSE correction scheme in Ref. 110. All values are in eV.

	absolute (non-relativistic)	absolute (relativistic)	relative
G_0W_0 -BSE@PBEh45	0.94	0.74	0.84
G_0W_0 -BSE/TDA@PBEh45	0.93	0.73	0.84
G_0W_0 -BSE/TDA@PBEh45 (Ref. 78)	0.81	0.62	0.67
TDDFT@PBE0	11.68	11.54	0.91
TDDFT@BHandHLYP	1.99	1.74	0.59
EOM-MBPT2	3.42	3.70	0.28
EOM-CCSD	3.11	3.40	0.26

We next examine the ability of the energy-specific GW -BSE approach to predict K -edge core excitation energies. Mean absolute errors (MAEs) of 31 excited states from 7 small molecules obtained from different computational methods are tabulated in Table II. As shown in Refs. 78, 116–118, G_0W_0 @PBEh45 is a good choice for calculating core-level binding energies, with errors of ~ 0.3 eV on the published datasets. Our G_0W_0 -BSE/TDA@PBEh45 results for K -edge excitation energies exhibit errors around 0.7 eV⁷⁸ and generally agree well with literature values in Ref. 78. The small differences from Ref 78 (around 0.1 eV) may originate from different treatments of relativistic effects and core-level orbitals described by numerical atomic orbitals (NAOs) in FHI-aims compared to Gaussian-type orbitals (GTOs) in PySCF. For K -edge excitation energies of these molecules obtained at G_0W_0 -BSE@PBEh45, the Tamm-Dancoff approximation incurs minimal additional error—both TDA and full BSE exhibit errors around 0.8 eV for predicting both absolute

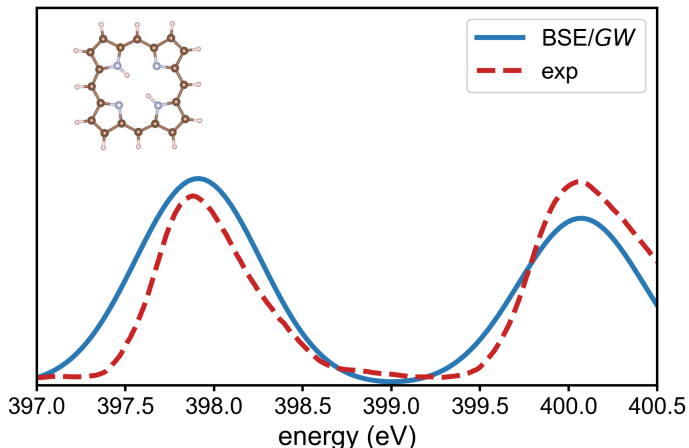


FIG. 1. XAS spectrum of N1s in porphine calculated with G_0W_0 -BSE@PBEh45 compared to experiment reference¹²⁴. The height of the calculated spectrum is scaled to that of experiment spectrum.

and relative K -edge excitation energies. With relativistic corrections, however, the errors of BSE for absolute K -edge excitation energies are reduced by more than 0.1 eV.

With an optimal functional BHandHLYP, the error of TDDFT for absolute K -edge excitation energies is around 2 eV, although TDDFT based on conventional functional PBE0 gives extremely high errors due to the delocalization error and the lack of screening effect¹²⁷. Two EOM approaches predict accurate relative K -edge excitation energies with errors around 0.2 eV. However, the errors of EOM approaches for absolute K -edge excitation energies are relatively large. In addition, the description at CCSD level can be insufficient for core-level excitations, for example, as shown in Ref. 118, high-order approaches such as CCSD(T) are needed to predict accurate core-level binding energies.

TABLE III. K -edge excitation energies of porphine obtained from BSE and BSE/TDA based on G_0W_0 @PBEh45 compared to experiments. aug-cc-pCVTZ/cc-pVDZ/aug-cc-pVDZ basis sets were used for the N, C, H atoms. Relativistic effects were considered using a post- GW -BSE correction scheme in Ref. 110. All values are in eV.

	exp ¹²⁸	exp ¹²⁴	BSE	BSE/TDA
A ₀	398.2	397.90	397.91	397.92
A ₄	400.3	400.00	400.07	400.08

We also applied the energy-specific GW -BSE approach to calculate N 1s K -edge excitation

energies of porphine. The energies thus obtained (G_0W_0 -BSE@PBEh45) are shown in Table III, and a simulated X-ray absorption spectrum is shown in Fig. 1 alongside the experimental spectrum from Ref. 124. Remarkably, the errors for both A_0 and A_4 K -edge excitation energies compared to the experiments in Refs. 123,124 are only 0.1 ~ 0.3 eV. In addition to its excellent, though perhaps fortuitous, accuracy in this case, the actual energy-specific BSE calculation was inexpensive. With a 48-CPU¹²⁹ node, the time required to converge 20 roots was 109 minutes (no TDA) and 3 minutes (with TDA). The computational bottleneck in the entire process was by a large margin the GW step, which uses the contour deformation technique to obtain accurate core-level QP energies but suffers from $O(N^5)$ scaling. Hopefully, the development of an appropriate Green's function embedding scheme^{101,103,130,131} will reduce the cost of the GW step in the future.

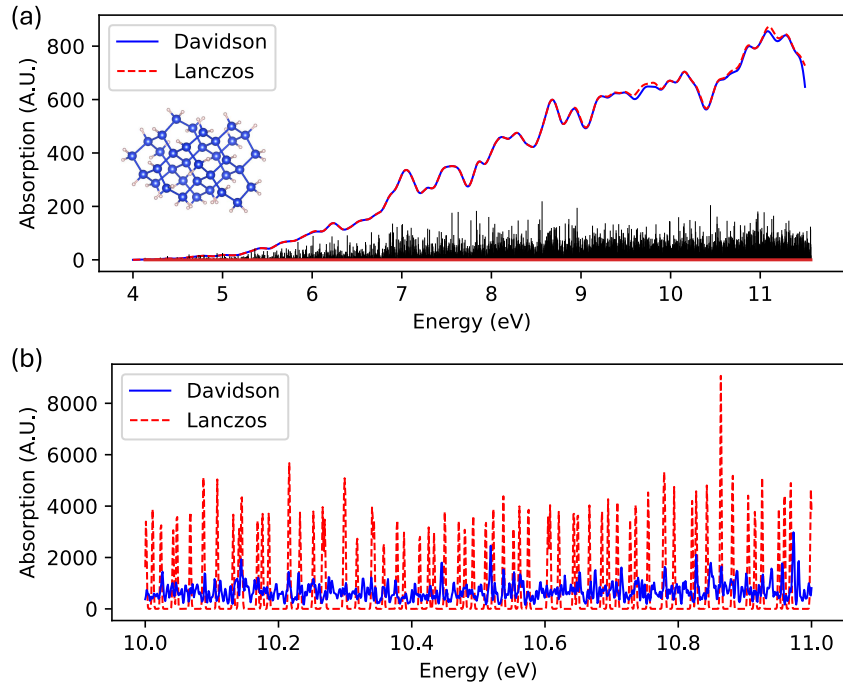


FIG. 2. Valence optical spectrum of the silicon nanocluster $\text{Si}_{35}\text{H}_{44}$ obtained from G_0W_0 -BSE@PBE0 with energy-specific Davidson and Lanczos algorithms. (a) Plot of both spectra with a broadening of 0.05 eV. Scaled oscillator strengths are shown in black. (b) Zoomed-in view with a much narrower broadening of 0.001 eV.

C. Valence Spectrum of Silicon Nanoclusters

We also applied the sliding window technique of Section II B 3 to calculate the optical absorption spectrum of the silicon nanocluster $\text{Si}_{35}\text{H}_{44}$ with GW -BSE. The truncated MO space of this system contains 92 occupied and 502 virtual orbitals, and the problem dimension is $92 \times 502 = 46,184$. The valence spectrum contains a very large number of densely spaced, nearly degenerate states; the energy of the 5000th lowest state is only ~ 11.5 eV. The optical absorption spectrum thus obtained is shown in Fig. 2. The sliding window technique described in Section II B 3 was chosen due to the need to converge a very large number of excited states without advance knowledge of the convergence behavior for the problem. Aside from this convenience, the technique appears to be rather efficient in terms of computational cost. When the solver moves up to a higher energy window, the Ritz vectors in that window are already orthogonal to transition amplitudes previously converged in lower energy windows. Because each energy window contains only 40 Ritz values, updates to the search space are smaller but more frequent than in Algorithm 1. In our experiments, this sometimes significantly reduces the number of trial vectors necessary to converge a given number of states. The whole calculation took about 6 hr 40 min on the same 48-CPU node. The maximum memory usage was 117 GB, most of which comprised the Cholesky-decomposed ERIs required to compute the action of v and W on transition vectors. With the maximum search space size set to 10,000, deflation occurred three times; the total number of matrix-vector products was about 40,000.

Remarkably, the optical absorption spectra from the Lanczos and Davidson algorithms agree very well, even though the Lanczos calculation took only 12 minutes (3% of the time for Davidson) on the same 48-CPU node. Since the excited states of this system are so densely spaced, precise transition densities are apparently irrelevant if one is interested only in the absorption spectrum. However, a closeup of the two optical spectra in Fig. 2(b), this time with a broadening of 0.001 eV, shows how the Lanczos algorithm has not converged individual Ritz values. Thus, the state-wise convergence guarantee provided by the Davidson algorithm is still valuable if one needs to analyze the character of individual excited states.

V. CONCLUSIONS

In summary, we present an energy-specific BSE approach for efficient optical spectrum calculations of high-lying excited states and wide energy ranges. In the energy-specific GW -BSE approach, trial vectors targeting excitation energies above the predefined energy threshold are constructed for the Davidson algorithm, then the subspace is expanded with new trial vectors associated with transitions above the target energy threshold. To calculate optical spectra over a wide energy range, energy-specific GW -BSE can be applied to multiple small energy windows, where trial vectors orthogonal to the true eigenvectors solved preceding energy windows are constructed for the subsequent energy window to accelerate the convergence of the Davidson algorithm. For K -edge excitation energies of small molecules and porphine, the energy-specific G_0W_0 -BSE@PBEh45 approach provides good accuracy with errors around 0.8 eV and high efficiency. For the silicon nanoclusters, the energy-specific G_0W_0 -BSE@PBE0 approach is capable of computing the optical spectra in a wide energy range up to 11.5 eV, which involves 5000 excited states. This work expands the applicability of the GW -BSE formalism for computing excited states of large systems.

SUPPORTING INFORMATION

See the Supporting Information for K -edge excitation energies of small molecules obtained from G_0W_0 -BSE@PBEh45 with different basis sets, K -edge excitation energies and oscillator strengths of porphine calculated with G_0W_0 -BSE@PBEh45, excitation energies of silicon nanoclusters obtained from G_0W_0 -BSE@PBE0.

ACKNOWLEDGMENTS

This work was supported by the Air Force Office of Scientific Research under award number FA9550-24-1-0096 (J. L. and T. Z.). C. H. acknowledges support from the National Science Foundation Engines Development Award: Advancing Quantum Technologies (CT) under award number 2302908. We thank Troy Van Voorhis for inspiring discussion.

DATA AVAILABILITY STATEMENT

The data that support the findings of this study are available from the corresponding author upon reasonable request.

REFERENCES

- ¹D. Rappoport and F. Furche, *J. Am. Chem. Soc.* **126**, 1277 (2004).
- ²S. Zhang, S. Sun, M. Zhou, L. Wang, and B. Zhang, *Sci. Rep.* **7**, 43419 (2017).
- ³T. Zhu and T. Van Voorhis, *J. Phys. Chem. C* **120**, 19987 (2016).
- ⁴T. Zhu, T. Van Voorhis, and P. de Silva, in *Handbook of Materials Modeling : Methods: Theory and Modeling*, edited by W. Andreoni and S. Yip (Springer International Publishing, Cham, 2018) pp. 1–31.
- ⁵T. Zhu and T. Van Voorhis, *J. Phys. Chem. C* **123**, 10311 (2019).
- ⁶M. T. Frederick, V. A. Amin, N. K. Swenson, A. Y. Ho, and E. A. Weiss, *Nano Lett.* **13**, 287 (2013).
- ⁷S. V. Kilina, P. K. Tamukong, and D. S. Kilin, *Acc. Chem. Res.* **49**, 2127 (2016).
- ⁸E. Runge and E. K. U. Gross, *Phys. Rev. Lett.* **52**, 997 (1984).
- ⁹M. E. Casida, in *Recent Advances in Density Functional Methods*, Recent Advances in Computational Chemistry, Vol. Volume 1 (WORLD SCIENTIFIC, 1995) pp. 155–192.
- ¹⁰C. A. Ullrich, *Time-Dependent Density-Functional Theory: Concepts and Applications* (OUP Oxford, 2011).
- ¹¹R. E. Stratmann, G. E. Scuseria, and M. J. Frisch, *J. Chem. Phys.* **109**, 8218 (1998).
- ¹²F. Furche and R. Ahlrichs, *J. Chem. Phys.* **117**, 7433 (2002).
- ¹³F. Sottile, F. Bruneval, A. G. Marinopoulos, L. K. Dash, S. Botti, V. Olevano, N. Vast, A. Rubio, and L. Reining, *Int. J. Quantum Chem.* **102**, 684 (2005).
- ¹⁴M. E. Casida, *J. Mol. Struct. THEOCHEM. Time-Dependent Density-Functional Theory for Molecules and Molecular Solids*, **914**, 3 (2009).
- ¹⁵A. D. Laurent and D. Jacquemin, *Int. J. Quantum Chem.* **113**, 2019 (2013).
- ¹⁶E. Brémond, M. Savarese, C. Adamo, and D. Jacquemin, *J. Chem. Theory Comput.* **14**, 3715 (2018).

- ¹⁷R. Sarkar, M. Boggio-Pasqua, P.-F. Loos, and D. Jacquemin, *J. Chem. Theory Comput.* **17**, 1117 (2021).
- ¹⁸Y. Jin, V. W.-z. Yu, M. Govoni, A. C. Xu, and G. Galli, *J. Chem. Theory Comput.* **19**, 8689 (2023).
- ¹⁹A. Dreuw, J. L. Weisman, and M. Head-Gordon, *J. Chem. Phys.* **119**, 2943 (2003).
- ²⁰D. J. Tozer, *J. Chem. Phys.* **119**, 12697 (2003).
- ²¹D. Hait and M. Head-Gordon, *J. Phys. Chem. Lett.* **12**, 4517 (2021).
- ²²D. Hait, K. J. Oosterbaan, K. Carter-Fenk, and M. Head-Gordon, *J. Chem. Phys.* **156**, 201104 (2022).
- ²³H. van Aggelen, Y. Yang, and W. Yang, *Phys. Rev. A* **88**, 030501 (2013).
- ²⁴Y. Yang, H. van Aggelen, and W. Yang, *J. Chem. Phys.* **139**, 224105 (2013).
- ²⁵Y. Yang, D. Peng, J. Lu, and W. Yang, *J. Chem. Phys.* **141**, 124104 (2014).
- ²⁶Y. Yang, D. Peng, E. R. Davidson, and W. Yang, *J. Phys. Chem. A* **119**, 4923 (2015).
- ²⁷Y. Yang, A. Dominguez, D. Zhang, V. Lutsker, T. A. Niehaus, T. Frauenheim, and W. Yang, *J. Chem. Phys.* **146**, 124104 (2017).
- ²⁸J. Li, J. Yu, Z. Chen, and W. Yang, *J. Phys. Chem. A* **127**, 7811 (2023).
- ²⁹J. Li, Z. Chen, and W. Yang, *J. Phys. Chem. Lett.* **13**, 894 (2022).
- ³⁰J. Li, Y. Jin, J. Yu, W. Yang, and T. Zhu, *J. Phys. Chem. Lett.* **15**, 2757 (2024).
- ³¹J. Li, Y. Jin, J. Yu, W. Yang, and T. Zhu, *J. Chem. Theory Comput.* **20**, 7979 (2024).
- ³²K. J. Oosterbaan, A. F. White, and M. Head-Gordon, *J. Chem. Theory Comput.* **15**, 2966 (2019).
- ³³K. Carter-Fenk and M. Head-Gordon, *Phys. Chem. Chem. Phys.* **24**, 26170 (2022).
- ³⁴P.-F. Loos, M. Boggio-Pasqua, A. Scemama, M. Caffarel, and D. Jacquemin, *J. Chem. Theory Comput.* **15**, 1939 (2019).
- ³⁵P.-F. Loos, M. Comin, X. Blase, and D. Jacquemin, *J. Chem. Theory Comput.* **17**, 3666 (2021).
- ³⁶P.-F. Loos, D. A. Matthews, F. Lipparini, and D. Jacquemin, *J. Chem. Phys.* **154**, 221103 (2021).
- ³⁷P.-F. Loos and D. Jacquemin, *J. Comput. Chem.* **45**, 1791 (2024).
- ³⁸P. Michalak and M. Lesiuk, *J. Chem. Theory Comput.* **20**, 8970 (2024).
- ³⁹N. O. C. Winter, N. K. Graf, S. Leutwyler, and C. Hättig, *Phys. Chem. Chem. Phys.* **15**, 6623 (2013).
- ⁴⁰P.-F. Loos, A. Scemama, A. Blondel, Y. Garniron, M. Caffarel, and D. Jacquemin, *J. Chem. Theory Comput.* **14**, 4360 (2018).
- ⁴¹I. M. Mazin and A. Y. Sokolov, *J. Chem. Theory Comput.* **19**, 4991 (2023).

- ⁴²R. Maier, M. Bauer, and A. Dreuw, *J. Chem. Phys.* **159**, 014104 (2023).
- ⁴³N. Sülzner and C. Hättig, *J. Chem. Theory Comput.* **20**, 2462 (2024).
- ⁴⁴E. E. Salpeter and H. A. Bethe, *Phys. Rev.* **84**, 1232 (1951).
- ⁴⁵L. J. Sham and T. M. Rice, *Phys. Rev.* **144**, 708 (1966).
- ⁴⁶W. Hanke and L. J. Sham, *Phys. Rev. Lett.* **43**, 387 (1979).
- ⁴⁷L. Hedin, *Phys. Rev.* **139**, A796 (1965).
- ⁴⁸R. M. Martin, L. Reining, and D. M. Ceperley, *Interacting Electrons* (Cambridge University Press, 2016).
- ⁴⁹X. Blase and C. Attaccalite, *Appl. Phys. Lett.* **99**, 171909 (2011).
- ⁵⁰D. Jacquemin, I. Duchemin, and X. Blase, *Mol. Phys.* **114**, 957 (2016).
- ⁵¹D. Jacquemin, I. Duchemin, and X. Blase, *J. Phys. Chem. Lett.* **8**, 1524 (2017).
- ⁵²C. Azarias, I. Duchemin, X. Blase, and D. Jacquemin, *J. Chem. Phys.* **146**, 034301 (2017).
- ⁵³T. Rangel, S. M. Hamed, F. Bruneval, and J. B. Neaton, *J. Chem. Phys.* **146**, 194108 (2017).
- ⁵⁴E. Monino and P.-F. Loos, *J. Chem. Theory Comput.* **17**, 2852 (2021).
- ⁵⁵Y. Cho, S. J. Bintrim, and T. C. Berkelbach, *J. Chem. Theory Comput.* **18**, 3438 (2022).
- ⁵⁶C. A. McKeon, S. M. Hamed, F. Bruneval, and J. B. Neaton, *J. Chem. Phys.* **157**, 074103 (2022).
- ⁵⁷J. Li, Y. Jin, N. Q. Su, and W. Yang, *J. Chem. Phys.* **156**, 154101 (2022).
- ⁵⁸J. Li, D. Golze, and W. Yang, *J. Chem. Theory Comput.* **18**, 6637 (2022).
- ⁵⁹C. Vorwerk and G. Galli, *Phys. Rev. Mater.* **7**, 033801 (2023).
- ⁶⁰X. Zhang, J. A. Leveillee, and A. Schleife, *Phys. Rev. B* **107**, 235205 (2023).
- ⁶¹J. B. Haber, D. Y. Qiu, F. H. da Jornada, and J. B. Neaton, *Phys. Rev. B* **108**, 125118 (2023).
- ⁶²N. Rauwolf, W. Klopper, and C. Holzer, *J. Chem. Phys.* **160**, 061101 (2024).
- ⁶³J. Wu, B. Hou, W. Li, Y. He, and D. Y. Qiu, *Phys. Rev. B* **110**, 075133 (2024).
- ⁶⁴R. Zhou, Y. Yao, V. Blum, X. Ren, and Y. Kanai, arXiv preprint arXiv:2406.11122 (2024).
- ⁶⁵X. Blase, I. Duchemin, and D. Jacquemin, *Chem. Soc. Rev.* **47**, 1022 (2018).
- ⁶⁶X. Blase, I. Duchemin, D. Jacquemin, and P.-F. Loos, *J. Phys. Chem. Lett.* **11**, 7371 (2020).
- ⁶⁷P. Hohenberg and W. Kohn, *Phys. Rev.* **136**, B864 (1964).
- ⁶⁸W. Kohn and L. J. Sham, *Phys. Rev.* **140**, A1133 (1965).
- ⁶⁹R. G. Parr and Y. Weitao, *Density-Functional Theory of Atoms and Molecules* (Oxford University Press, 1989).
- ⁷⁰K. Krause and W. Klopper, *J. Comput. Chem.* **38**, 383 (2017).
- ⁷¹O. Çaylak and B. Baumeier, *J. Chem. Theory Comput.* **17**, 4891 (2021).

- ⁷²C. Venturella, C. Hillenbrand, J. Li, and T. Zhu, *J. Chem. Theory Comput.* **20**, 143 (2024).
- ⁷³C. Venturella, J. Li, C. Hillenbrand, X. L. Peralta, J. Liu, and T. Zhu, arXiv preprint arXiv:2407.20384 (2024).
- ⁷⁴T. Biswas and A. K. Singh, arXiv preprint arXiv:2401.17831 (2024).
- ⁷⁵J. D. Elliott, N. Colonna, M. Marsili, N. Marzari, and P. Umari, *J. Chem. Theory Comput.* **15**, 3710 (2019).
- ⁷⁶P.-F. Loos and P. Romaniello, *J. Chem. Phys.* **156**, 164101 (2022).
- ⁷⁷R. Orlando, P. Romaniello, and P.-F. Loos, in *Advances in Quantum Chemistry*, Vol. 88, edited by P. E. Hoggan (Academic Press, 2023) pp. 183–211.
- ⁷⁸Y. Yao, D. Golze, P. Rinke, V. Blum, and Y. Kanai, *J. Chem. Theory Comput.* 10.1021/acs.jctc.1c01180 (2022).
- ⁷⁹M. Kick, E. Alexander, A. Beiersdorfer, and T. Van Voorhis, *Nat. Commun.* **15**, 8001 (2024).
- ⁸⁰D. Neuhauser, *J. Chem. Phys.* **93**, 2611 (1990).
- ⁸¹M. R. Wall and D. Neuhauser, *J. Chem. Phys.* **102**, 8011 (1995).
- ⁸²N. C. Bradbury, M. Nguyen, J. R. Caram, and D. Neuhauser, *J. Chem. Phys.* **157**, 10.1063/5.0100213 (2022).
- ⁸³N. C. Bradbury, T. Allen, M. Nguyen, K. Z. Ibrahim, and D. Neuhauser, *J. Chem. Phys.* **158**, 10.1063/5.0146555 (2023).
- ⁸⁴W. Liang, S. A. Fischer, M. J. Frisch, and X. Li, *J. Chem. Theory Comput.* **7**, 3540 (2011).
- ⁸⁵B. Peng, P. J. LeStrange, J. J. Goings, M. Caricato, and X. Li, *J. Chem. Theory Comput.* **11**, 4146 (2015).
- ⁸⁶P. J. LeStrange, P. D. Nguyen, and X. Li, *J. Chem. Theory Comput.* **11**, 2994 (2015).
- ⁸⁷J. M. Kasper, D. B. Williams-Young, E. Vecharynski, C. Yang, and X. Li, *J. Chem. Theory Comput.* **14**, 2034 (2018).
- ⁸⁸Z. Bai and R.-C. Li, *SIAM J. Matrix Anal. Appl.* **33**, 1075 (2012).
- ⁸⁹M. Shao, F. H. da Jornada, C. Yang, J. Deslippe, and S. G. Louie, *Linear Algebra Its Appl.* **488**, 148 (2016).
- ⁹⁰S. K. Ghosh and P. K. Chattaraj, *Concepts and Methods in Modern Theoretical Chemistry: Electronic Structure and Reactivity* (CRC Press, 2016).
- ⁹¹D. Zhang, S. N. Steinmann, and W. Yang, *J. Chem. Phys.* **139**, 154109 (2013).
- ⁹²S. J. Bintrim and T. C. Berkelbach, *J. Chem. Phys.* **156**, 044114 (2022).
- ⁹³D. Rocca, D. Lu, and G. Galli, *J. Chem. Phys.* **133**, 164109 (2010).

- ⁹⁴I. Duchemin, T. Deutsch, and X. Blase, *Phys. Rev. Lett.* **109**, 167801 (2012).
- ⁹⁵C. Faber, P. Boulanger, I. Duchemin, C. Attaccalite, and X. Blase, *J. Chem. Phys.* **139**, 194308 (2013).
- ⁹⁶M. Shao, F. H. da Jornada, L. Lin, C. Yang, J. Deslippe, and S. G. Louie, *SIAM J. Matrix Anal. Appl.* **39**, 683 (2018).
- ⁹⁷E. Vecharynski, J. Brabec, M. Shao, N. Govind, and C. Yang, *Comput. Phys. Commun.* **221**, 42 (2017).
- ⁹⁸Users of LAPACK may find it convenient to use `dsygv`.
- ⁹⁹A rank-revealing QR decomposition is convenient since it allows one to discard negligible components of \mathbf{Q} . As \mathbf{U} grows large, it may be necessary to orthogonalize against \mathbf{U} before and after QR to avoid restarts.
- ¹⁰⁰fcDMFT library, <https://github.com/ZhuGroup-Yale/fcdmft> (2024).
- ¹⁰¹T. Zhu, Z.-H. Cui, and G. K.-L. Chan, *J. Chem. Theory Comput.* **16**, 141 (2020).
- ¹⁰²Z.-H. Cui, T. Zhu, and G. K.-L. Chan, *J. Chem. Theory Comput.* **16**, 119 (2020).
- ¹⁰³T. Zhu and G. K.-L. Chan, *Phys. Rev. X* **11**, 021006 (2021).
- ¹⁰⁴Q. Sun, T. C. Berkelbach, N. S. Blunt, G. H. Booth, S. Guo, Z. Li, J. Liu, J. D. McClain, E. R. Sayfutyarova, S. Sharma, S. Wouters, and G. K.-L. Chan, *WIREs Comput. Mol. Sci.* **8**, e1340 (2018).
- ¹⁰⁵Q. Sun, X. Zhang, S. Banerjee, P. Bao, M. Barbry, N. S. Blunt, N. A. Bogdanov, G. H. Booth, J. Chen, Z.-H. Cui, J. J. Eriksen, Y. Gao, S. Guo, J. Hermann, M. R. Hermes, K. Koh, P. Koval, S. Lehtola, Z. Li, J. Liu, N. Mardirossian, J. D. McClain, M. Motta, B. Mussard, H. Q. Pham, A. Pulkin, W. Purwanto, P. J. Robinson, E. Ronca, E. R. Sayfutyarova, M. Scheurer, H. F. Schurkus, J. E. T. Smith, C. Sun, S.-N. Sun, S. Upadhyay, L. K. Wagner, X. Wang, A. White, J. D. Whitfield, M. J. Williamson, S. Wouters, J. Yang, J. M. Yu, T. Zhu, T. C. Berkelbach, S. Sharma, A. Y. Sokolov, and G. K.-L. Chan, *J. Chem. Phys.* **153**, 024109 (2020).
- ¹⁰⁶T. Zhu and G. K.-L. Chan, *J. Chem. Theory Comput.* **17**, 727 (2021).
- ¹⁰⁷J. Lei and T. Zhu, *J. Chem. Phys.* **157**, 214114 (2022).
- ¹⁰⁸G. L. Stoychev, A. A. Auer, and F. Neese, *J. Chem. Theory Comput.* **13**, 554 (2017).
- ¹⁰⁹B. P. Pritchard, D. Altarawy, B. Didier, T. D. Gibson, and T. L. Windus, *J. Chem. Inf. Model.* **59**, 4814 (2019).
- ¹¹⁰L. Keller, V. Blum, P. Rinke, and D. Golze, *J. Chem. Phys.* **153**, 114110 (2020).
- ¹¹¹F. Weigend and R. Ahlrichs, *Phys. Chem. Chem. Phys.* **7**, 3297 (2005).

- ¹¹²M. J. Frisch, G. W. Trucks, H. B. Schlegel, G. E. Scuseria, M. A. Robb, J. R. Cheeseman, G. Scalmani, V. Barone, G. A. Petersson, H. Nakatsuji, X. Li, M. Caricato, A. V. Marenich, J. Bloino, B. G. Janesko, R. Gomperts, B. Mennucci, H. P. Hratchian, J. V. Ortiz, A. F. Izmaylov, J. L. Sonnenberg, D. Williams-Young, F. Ding, F. Lipparini, F. Egidi, J. Goings, B. Peng, A. Petrone, T. Henderson, D. Ranasinghe, V. G. Zakrzewski, J. Gao, N. Rega, G. Zheng, W. Liang, M. Hada, M. Ehara, K. Toyota, R. Fukuda, J. Hasegawa, M. Ishida, T. Nakajima, Y. Honda, O. Kitao, H. Nakai, T. Vreven, K. Throssell, J. A. Montgomery, Jr., J. E. Peralta, F. Ogliaro, M. J. Bearpark, J. J. Heyd, E. N. Brothers, K. N. Kudin, V. N. Staroverov, T. A. Keith, R. Kobayashi, J. Normand, K. Raghavachari, A. P. Rendell, J. C. Burant, S. S. Iyengar, J. Tomasi, M. Cossi, J. M. Millam, M. Klene, C. Adamo, R. Cammi, J. W. Ochterski, R. L. Martin, K. Morokuma, O. Farkas, J. B. Foresman, and D. J. Fox, Gaussian16 Revision a.03 (2016), gaussian Inc. Wallingford CT.
- ¹¹³T. H. Dunning, *J. Chem. Phys.* **90**, 1007 (1989).
- ¹¹⁴D. E. Woon and T. H. Dunning, Jr., *J. Chem. Phys.* **103**, 4572 (1995).
- ¹¹⁵M. J. van Setten, F. Weigend, and F. Evers, *J. Chem. Theory Comput.* **9**, 232 (2013).
- ¹¹⁶D. Golze, J. Wilhelm, M. J. van Setten, and P. Rinke, *J. Chem. Theory Comput.* **14**, 4856 (2018).
- ¹¹⁷D. Golze, L. Keller, and P. Rinke, *J. Phys. Chem. Lett.* **11**, 1840 (2020).
- ¹¹⁸J. Li, Y. Jin, P. Rinke, W. Yang, and D. Golze, *J. Chem. Theory Comput.* **18**, 7570 (2022).
- ¹¹⁹A. D. Becke, *J. Chem. Phys.* **98**, 5648 (1993).
- ¹²⁰C. Lee, W. Yang, and R. G. Parr, *Phys. Rev. B* **37**, 785 (1988).
- ¹²¹S. Grimme, J. Antony, S. Ehrlich, and H. Krieg, *J. Chem. Phys.* **132**, 154104 (2010).
- ¹²²P. C. Hariharan and J. A. Pople, *Theoret. Chim. Acta* **28**, 213 (1973).
- ¹²³K. Diller, F. Klappenberger, F. Allegretti, A. C. Papageorgiou, S. Fischer, A. Wiengarten, S. Joshi, K. Seufert, D. Ćecija, W. Auwärter, and J. V. Barth, *J. Chem. Phys.* **138**, 154710 (2013).
- ¹²⁴S. A. Krasnikov, N. N. Sergeeva, M. M. Brzhezinskaya, A. B. Preobrajenski, Y. N. Sergeeva, N. A. Vinogradov, A. A. Cafolla, M. O. Senge, and A. S. Vinogradov, *J. Phys.: Condens. Matter* **20**, 235207 (2008).
- ¹²⁵M. V. Wolkin, J. Jorne, P. M. Fauchet, G. Allan, and C. Delerue, *Phys. Rev. Lett.* **82**, 197 (1999).
- ¹²⁶J. Brabec, L. Lin, M. Shao, N. Govind, C. Yang, Y. Saad, and E. G. Ng, *J. Chem. Theory Comput.* **11**, 5197 (2015).
- ¹²⁷J. Yu, Y. Mei, Z. Chen, and W. Yang, arXiv preprint arXiv:2406.06345 (2024).

¹²⁸G. Polzonetti, V. Carravetta, G. Iucci, A. Ferri, G. Paolucci, A. Goldoni, P. Parent, C. Laffon, and M. V. Russo, *Chem. Phys.* **296**, 87 (2004).

¹²⁹2 x Intel[®] Xeon[®] Platinum 8268 CPU @ 2.90GHz.

¹³⁰J. Li and T. Zhu, *Faraday Discuss.* (2024).

¹³¹J. Li and T. Zhu, arXiv preprint arXiv:2406.07531 (2024).